Chalcogenide Letters Vol. 15, No. 9, Septembrie 2018, p. 441 - 449

MORPHOLOGICAL, STRUCTURAL, COMPOSITIONAL AND RAMAN CHARACTERIZATION OF ZnS_XSe_{1-X} THIN FILMS DEPOSITED BY QUASI-CLOSED VOLUME TECHNIQUE

M. E. POPA*
Department of Physical Sciences and Engineering, Alecu Russo Balty State University, Balty MD-3100, Republic of Moldova

ZnS_XSe_{1-X} (x = 0, 0.2, 0.4, 0.5, 0.6, 0.8 and 1.0) thin films were deposited onto glass substrates using thermal evaporation under vacuum technique, in a quasi-closed volume. By X-ray diffraction technique it was revealed that the obtained films are polycrystalline, having a cubic blende structure. The cubic lattice parameter, a, ranged from 5.658 nm (for x = 0) and 5.406 nm (for x = 1). The crystallite sizes decrease with increase of x from D = 20.0 nm to D = 13.4 nm. Scanning electron microscopy (SEM) and atomic force microscopy (AFM) reveal a columnar grain shape and a low roughness of the surface. The chemical composition of the ZnS_XSe_{1-X} obtained films were confirmed by energy-dispersive X-ray spectroscopy (EDX). The vibrational properties of the ZnS_xSe_{1-x} thin films are studied using Raman scattering measurements.

(Received July 2, 2018; Accepted September 6, 2018)

Keywords: Thin films, XRD, AFM, EDAX, Raman

1. Introduction

In recent years, zinc sulfide (ZnS), zinc selenide (ZnSe) and ternary alloys of type ZnS_xSe_{1-x}, in thin films, have attracted considerable attention due to their interesting electronic and optical characteristics such as wide energy band gap (2.70 eV for ZnSe [1-5] and 3.51 eV for ZnS [6], at room temperature), high transmission coefficient in visible spectral range, high chemical and thermal stability. Regarding ZnS_xSe_{1-x} alloys, as it is well known [7-11], the ZnS/ZnSe system has a complete miscibility in solid phase. As result, the interest in preparation and investigations of the physical properties of such materials is given by the possibility of continuously variation of these properties with variation of their chemical composition (the value of x). Also, ZnS_xSe_{1-x} type semiconductors combine the remarkable optical properties of ZnSe with notable thermal stability of ZnS. By varying the chemical composition (i.e. S/Se ratio in ZnS_xSe_{1-x} alloy), the characteristics parameters can be continuously changed. For example, the band-gap can be continuously tuned from a value of 2.0 eV up to 3.5 eV and, accordingly, the photoemission wavelength of the alloy. In this way, ZnS_xSe_{1-x} alloys thin films offer a large number of actual and promising applications including optoelectronic devices operating in blue-green spectral domain, magneto-electronic devices, electroluminescent light emitting panels, technology of transparent electronic devices, chemical sensors, spin electronics etc. [12-15]

In the literature, some information are presented regarding the uses of the ZnS_xSe_{1-x} thin films in different optoelectronic devices, such as light emitting diodes and lasers diodes [7, 16-21] or as component of the heterojunctions solar cells [9, 13, 22-27]. Regarding the environment protection, nanostructured ZnS_xSe_{1-x} thin films tend to be considered as an alternative material for producing window and buffer layers in photovoltaic applications, replacing widely used cadmium sulfide (CdS), which is considered toxic for environment [11].

On the other hand, a great variety of methods have been elaborated in order to prepare high-quality ZnS_xSe_{1-x} alloys in thin films, including chemical bath deposition [6], laser ablation [10], high-pressure sputtering [11], successive ionic layer adsorption and reaction (SILAR)

*Corresponding author: miheugpopa@yahoo.com

method [28] electrodeposition [29-31], molecular beam epitaxy [32], RF sputtering [33], and other.

In the present paper, we extensively present our research results regarding the structural, morphological and compositional properties of the ZnS_xSe_{1-x} ($0 < x < 1$) thin films, obtained by thermal evaporation under vacuum, in quasi-closed volume, of ZnS and ZnSe powders mixture, onto glass substrates.

2. Experimental details

In order to prepare ZnS_xSe_{1-x} thin films, an automatic VUP-5 [OAO, Selmi] vacuum installation were used. In the main vacuum compartment, a small quasi-closed chamber was placed around the tungsten evaporation source and the substrates holder. As starting materials, 99.99% purity ZnSe and ZnS powders (Sigma-Aldrich) were used. In order to obtain ZnS_xSe_{1-x} thin films having different x-ratio, the powders were weighted using a precision balance Secura 613-1S (Sartorius-Secura). In such way, values of x = 0 (pure ZnSe), 0.2, 0.4, 0.5, 0.6, 0.8 and 1.0 (pure ZnS) were achieved. Subsequently, the powders were mechanically mixed until a uniform color is obtained.

As substrates, 15x15 mm glass (Corning 1737f) slides were used. Before deposition, these substrates were cleaned using water diluted washing powder then, for 5 min. in acetone and for 10 min. in ethanol, using an ultrasonic bath (Bandelin Sonorex). Finally, the substrates were washed with deionized water and dried in nitrogen flux.

The distance between evaporation source and substrates holder were modified in the range 70 – 120 mm. In this range, no influence on the obtained films was noticed, these having uniform thicknesses. The films investigated in the present paper were obtained using 70 mm distance. During deposition, the substrates temperature were maintained at 300 K (room temperature) and the evaporator temperature ranges between 1300 K (at the beginning of deposition) and 1100 K (at the end). In this way, for different deposition times, thin films having thicknesses ranged between 0.2 and 1.0 μm were obtained. The film thickness was determined by a Fizeau interferometer Linnik MII-2 (LOMO) using monochromatic light (λ = 550 nm).

The crystalline structure of the obtained films were investigated by X-ray diffraction technique with a Shimadzu LABX XRD-6000 diffractometer, using CuKα radiation (λ = 1,5418Å) and in the 2θ range between 20 and 70 deg (working parameters were: I = 20 mA and U = 40kV).

The surface morphology of the obtained films was investigated by atomic force microscopy using a Q-Scope 250 microscope (Quesant Instrument Corporation).

Regarding the quantitative chemical composition of the ZnS_xSe_{1-x} thin films, these were studied by energy dispersive analysis of X-ray diffraction using a Jeol 7001 TTLS spectrometer.

Raman spectrums of the ZnS_xSe_{1-x} thin films were characterized by Micro-Raman spectrometer (HR800) under two excitation wavelengths of 532 nm and 785 nm.

3. Results and discussions

By X-ray diffraction it was found that the obtained ZnS_xSe_{1-x} thin films are crystalline having a cubic (zinc blende) structure highly oriented with (111) planes parallel to the substrates surface (Fig. 1). As can be easily observed from Fig. 1 and Table 1, the position of the (111) diffraction peak shift from 2θ = 27,30 deg (for x = 0) to 2θ = 28,61 deg (for x = 1). This shift is determined by the values of the lattice parameters determined by S/Se ratio in the films.

It is known that, in principle, the number of molecules in vapor phase, n, striking unit area of the substrate surface in time unit can be calculated using the expression [34]

$$p = nkt\,, \tag{1}$$

where p is the vapor pressure and T is the absolute temperature. The vapor pressure of ZnSe is higher than those of ZnS [**35**]. Consequently, at the same temperature, unequal numbers of ZnSe and ZnS molecules strike the substrate. On other hand, the formation of Zn-Se bonds in the final alloy is more favorable than Zn-S ones. During the film growth, this leads to a replacement of the selenium atoms by the sulphur ones. Accordingly, the lattice parameters will change.

The cubic lattice parameter, a, was calculated using the well known relation [36]

$$a = \frac{\lambda}{2\sin\theta}\sqrt{h^2 + k^2 + l^2}\ , \tag{2}$$

where *h*, *k* and *l* are Miller indexes of the used diffraction plane ((111), in our case), θ is the diffraction angle and λ is the X-ray wavelength (λ = 1.5418 Å). For our samples, the obtained values ranged between *a* = 5.658Å (for *x* = 0) and *a* = 5.406 Å (for *x* = 1) (Table 1). The obtained values for our pure ZnSe and ZnS thin films are similar with other presented in the literature, being very close to those obtained for bulk materials [37, 38].

Using the XRD patterns, the crystallite sizes, *D*, were calculated, using the Scherer formula [36]

$$D = \frac{0.9\lambda}{\beta\cos\theta}\ , \tag{3}$$

where β is the full width at half maximum (FWHM) of the (111) peaks and 0.9 is the most used value of the Scherer's constant (shape factor), *k*. For the studied samples, the obtained results, presented in Table 1, ranged between *D* = 20.0 nm (for *x* = 0) and *D* = 13.4 nm (for *x* = 1).

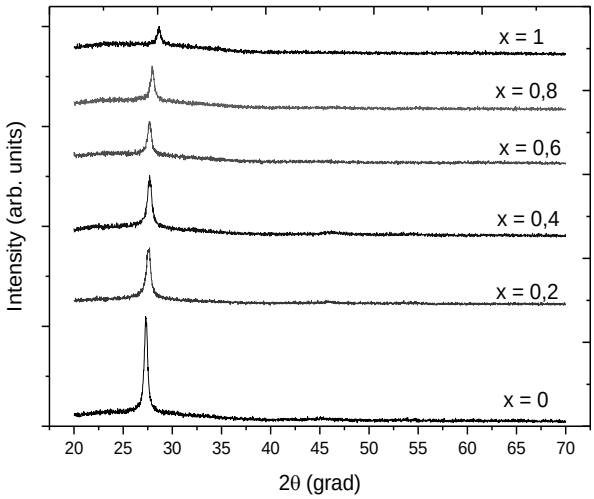

Fig. 1. *XRD patterns of studied ZnS_xSe_{1-x} thin films.*

We also verify the obey of the Vegard law [39], written as

$$a_{ZnS_xSe_{1-x}} = xa_{ZnS} + (1-x)a_{ZnSe}\quad , \tag{4}$$

where $a_{ZnS_xSe_{1-x}}$ is the lattice parameter of the ZnS_xSe_{1-x} sample and a_{ZnS} and a_{ZnSe} is the lattice parameters determined from XRD patterns, respectively 5.658 Å for ZnSe and 5.406 Å for ZnS. The result presented in Table 1 is in good agreement with those determined from XRD pattern. This means that the values of *x* in our ZnS_xSe_{1-x} thin films are correctly.

Table 1. The experimental values for the cubic structure of the studied ZnS_xSe_{1-x} thin films d – film thickness; d_{111} – interplanar distance corresponding to (111) planes; D – crystallite size; $a_{exp.}$ – cubic lattice parameter determined from XRD pattern; a_{Veg} – lattice parameter determined by Vegard law.

x	*d* (nm)	d_{111} (Å)	*D* (nm)	$a_{exp.}$ (Å)	a_{Veg} (Å)
0	550	3.27	20.0	5.658	–
0.2	670	3.25	18.9	5.634	5.607
0.4	780	3.23	17.6	5.586	5.557
0.5	520	3.21	16.5	5.559	5.532
0.6	410	3.19	15.5	5.529	5.507
0.8	220	3.16	14.5	5.473	5.456
1.0	410	3.12	13.4	5.406	–

Table 2. Atomic percentage of the elements as resulted from EDX analysis.

Compound	Zn (%)		S (%)		Se (%)		C (%)
	theor.	exper.	theor.	exper.	theor.	exper.	exper.
ZnS	50	52.2	50	46.0	-	-	1.8
$ZnS_{0.8}Se_{0.2}$	50	52.0	40	35.9	10	10.1	2.0
$ZnS_{0.6}Se_{0.4}$	50	51.6	30	27.7	20	18.9	1.8
$ZnS_{0.5}Se_{0.5}$	50	51.5	25	22.8	25	23.2	2.5
$ZnS_{0.4}Se_{0.6}$	50	50,9	20	19.1	30	28.2	2.4
$ZnS_{0.2}Se_{0.8}$	50	50.6	10	9.6	40	37.8	2.0
ZnSe	50	50.3	-	-	50	47.1	2.0

In order to additionally confirm this, chemical composition of the obtained films was performed by EDX. The obtained spectra, presented in Fig. 2, reveal the presence in the films of the expected chemical elements, respectively Zn, S and Se. The small amount of carbon, which is present in the spectra, is due to the glass substrates.

In Table 2, theoretical and experimental percentages of the chemical elements are presented. It can be clearly observed that the experimental data are very closely to the expected theoretical ones.

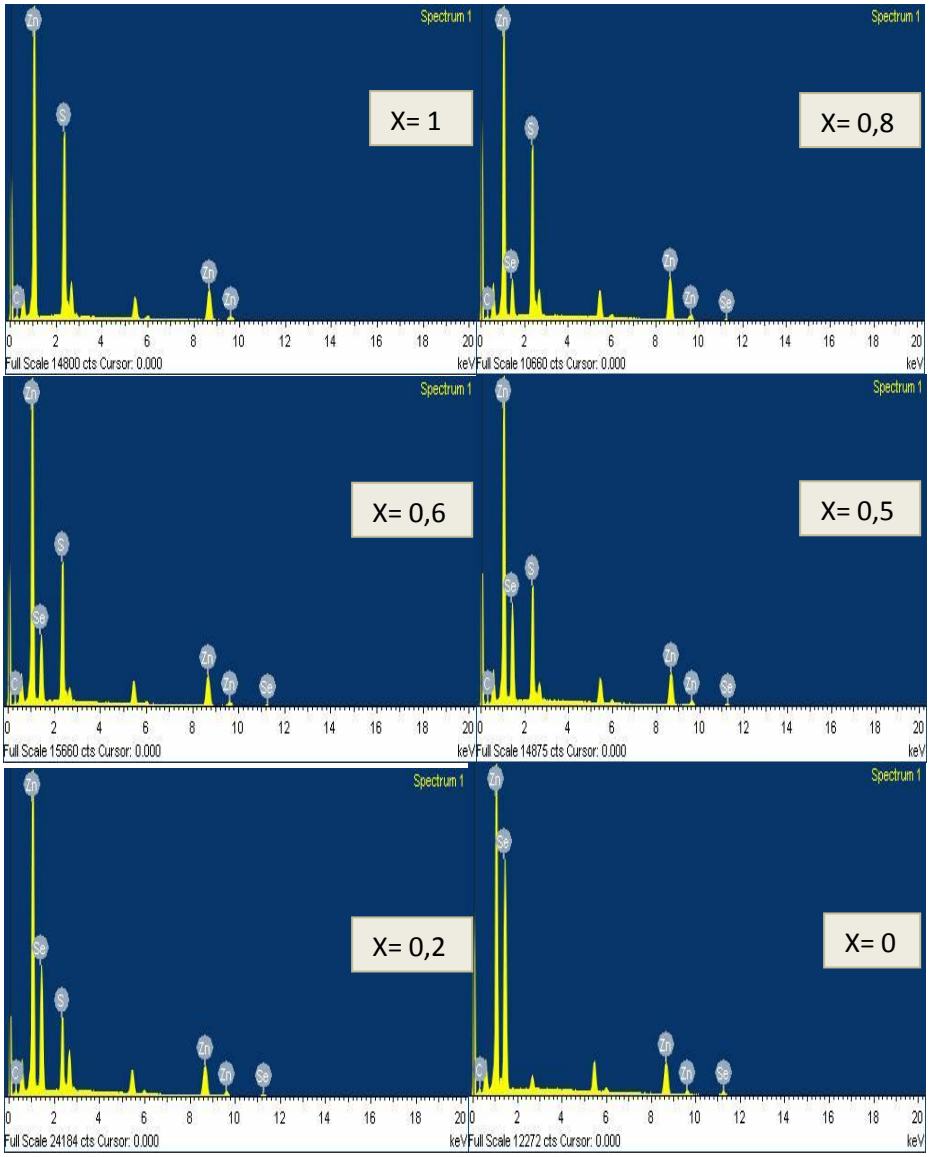

Fig. 2. EDX spectra for the ZnS_xSe_{1-x} studied samples.

In order to obtain additional information about the surface structure, SEM and AFM studies were performed. In Figs. 3 a and b can be observed that the crystallite sizes are small but these have uniform shapes and sizes. Also, the crystallites were grown perpendicular to substrates in a columnar manner. With increasing the sulphur content (value of x) and decreasing selenium content, the crystallite sizes decrease, as was also confirmed by XRD studies (Table 1). The decrease of the crystallite size strongly influences electronic transport properties of the studied films.

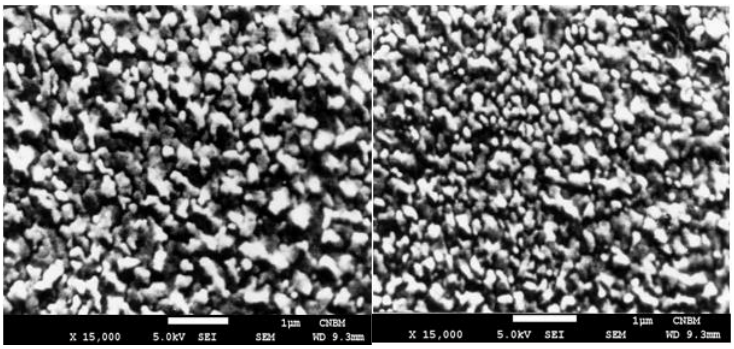

a) *b)*

Fig. 3. SEM images (12000 × magnification) of the surfaces for the $ZnS_{0.2}Se_{0.8}$ (a) and $ZnS_{0.8}Se_{0.2}$ (b) thin films.

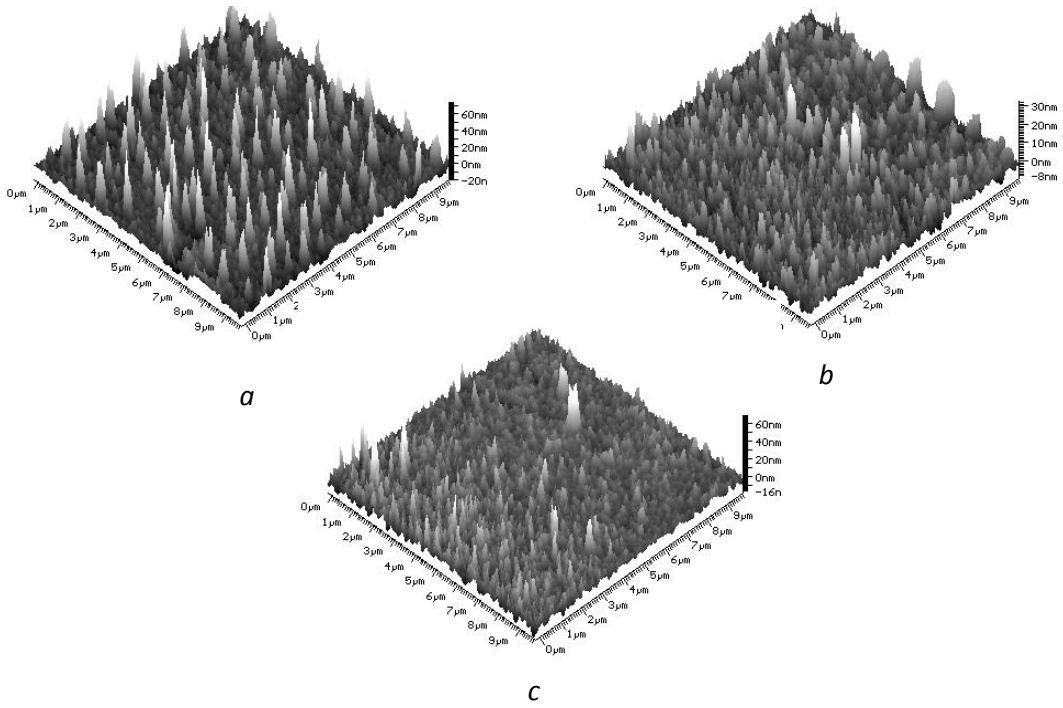

a *b* *c*

Fig. 4. AFM images of the $ZnS_{0.2}Se_{0.8}$ (a), $ZnS_{0.5}Se_{0.5}$ (b) and $ZnS_{0.8}Se_{0.2}$ (c) thin films.

In order to obtain additional information about the surface structure, AFM studies were performed. In Figs. 3 a-d can be observed that the crystallite sizes are small but these have uniform shapes and sizes. Also, the crystallites were grown perpendicular to substrates in a columnar manner. With increasing the sulphur content (value of x) and decreasing selenium content, the crystallite sizes decrease, as was also confirmed by XRD studies (Table 1). The decrease of the crystallite size strongly influences electronic transport properties of the studied films. Also, from AFM images, it can be observed that the surface roughness decrease with increasing of the sulphur content (Figs. 3).

The AFM studies also confirm the conclusions above (Figs. 4). Also, from AFM images, it can be observed that the surface roughness decrease with increasing of the sulphur content. The low roughness ranged between 60-70 nm and 0-20 nm for x = 1.

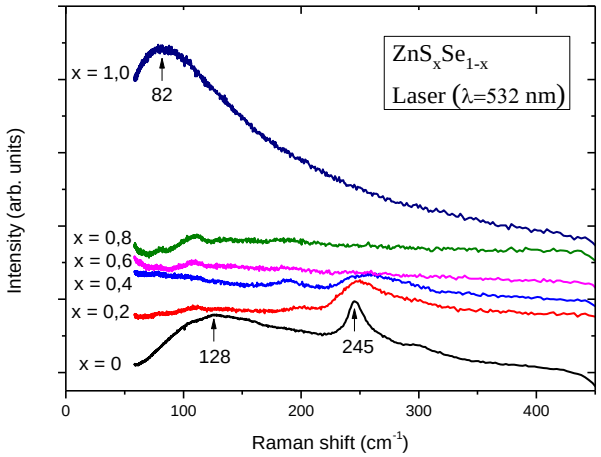

Fig. 5. Raman spectra of ZnS_xSe_{1-x} thin films.

In solid state physics, Raman spectrometry is used to characterize of materials in bulk and thin film form and is very sensitive to composition of the structure. It is a very pronounced and more technologically important spectroscopic technique to probe vibrational states of the crystals or semiconductor materials. In Fig. 5 are presented seven Raman spectra of thin ZnS_xSe_{1-x} thin films excited by laser with wavelength λ = 532 nm. In pure ZnSe it appears a peak at 245 cm^{-1}, which has a Lorentzian profile and is attributed to the LO_{ZnSe} phonon (longitudinal optical mode of ZnSe) and it is agrees with the published results [40-48]. It confirms the formation of single phase cubic (zinc blend) crystalline structure of ZnSe film deposited at room temperature on glass substrate. The second pic appears at about 128 cm^{-1} and is assigned to the $2TA_{ZnSe}$ (second transverse acoustic mode of ZnSe) and it is consistent with published results [46, 49]. With the increase in sulfur content in thin layers the intensity of both peaks diminishes. In pure ZnS appears a bit peack at the short Raman frequency of 82 cm^{-1} of the type E_2^1 and that represents a nonpolar mode of vibration and can be associated with vibrations of heavy Zn sublattice [50-52].

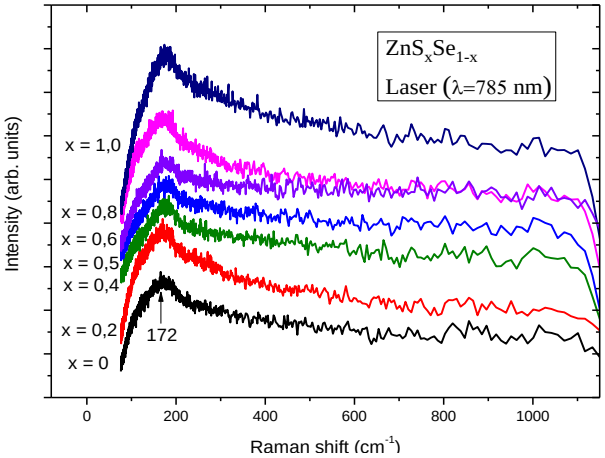

Fig. 6. Raman spectra of ZnS_xSe_{1-x} thin films

Fig. 6 shows the Raman spectra of thin ZnS_xSe_{1-x} thin films excited by the laser with wavelength λ = 785 nm. In all samples it appears a wide peack with the Raman frequency of 173 cm^{-1} who has a lorentzian profile. For pure ZnSe it is assigned to the phonon $2LA_{ZnSe}$ (second longitudinal acustic mode of ZnSe) [**49, 53**] and for pure ZnS this peak is assigned to the $2TA_{ZnS}$ phonon (second longitudinal optical mode of ZnS) [**54**].

Good knowledge of the vibration properties of the materials is crucial to the understanding of the transport properties and phonon interactions with the free carriers because they have great impact on optoelectronic device performance.

4. Conclusions

In the present paper are presented new results regarding the studies onto structural, morphological and chemical composition of the ZnS_xSe_{1-x} thin films, obtained by thermal evaporation in vacuum. The results show that the samples present a high crystallinity with small sizes crystallites having a zinc blende structure. Also the films surfaces present a low roughness. The obtained results demonstrate the possibility of using thermal evaporation under vacuum method as a cheap way for obtaining high quality films with possible applications in optoelectronic devices.

References

[1] G. I. Rusu, M. E. Popa, G. G. Rusu, Iulia N. Salaoru, Applied Surface Science **218**(1 – 4), 213 (2003).
[2] M. E. Popa, G. I. Rusu, Physics of Low – Dimensional Structures 7/8, 43 (2003).
[3] G. I. Rusu, V. Ciupina, M. E. Popa, G. Prodan, G. G. Rusu, C. Baban, Journal of Non-Crystalline Solids **352**, 1525 (2006).
[4] G. I. Rusu, M. Diciu, C. Pîrghie, M. E. Popa, Applied Surface Science **253**, 9500 (2007).
[5] M. E. Popa, G. I. Rusu, Optoelectron. Adv. Mat. **5**(8), 842 (2011).
[6] M. S. Shinde, P. B. Ahirrao , I. J. Patil, R. S. Patil, Indian Journal of Pure & Applied Physics, **49**, 765 (2011).
[7] D. S. Patil, D. K. Gautam, Physica B **344**, 140 (2004).
[8] Y. P. Venkata Subbaiah, P. Prathap, K. T. R. Reddy, D. Mangalaraj, K. Kim, Yi Junsin, Journal of Physics D: Applied Physics **40**, 3683 (2007).
[9] Y. P. Venkata Subbaiah, P. Prathap, K. T. Ramakrishna Reddy, R. W. Miles, J. Yi, Thin Solid Films **516**, 7060 (2008).
[10] M. Ambrico, G. Perna, D. Smaldone, C. Spezzacatena, V. Stagno, V. Capozzi, Semicond. Sci. Technol. **13**, 1446 (1998).
[11] A. Ganguly, S. Chaudhury, A. K. Pal, Journal of Physics D: Applied Physics **34**, 506 (2001).
[12] I. Shafiq, A. Sharif, L. C. Sing, Physica E **41**, 739 (2009).
[13] S. V. Sorokin, S. V. Gronin, I. V. Sedova, G. V. Klimko, E. A. Evropeitsev, M. V. Baidakova, A. A. Sitnikova, A. A. Toropov, S. V. Ivanov, Fizika i Tekhnika Poluprovodnikov **49**(8), 1024 (2015).
[14] Z. Wang, Y. Hong, C. Jiang, M. Safdar, J. He, Applied Physics Letters **101**, 253109 (2012).
[15] S. M. Shaban, N. M. Saeed, R. M. S. AL-Haddad, Indian Journal of Science and Technology **4**(4), (2011).
[16] T. Shirakawa, Materials Science and Engineering **B91** – 92, 470 (2002).
[17] D. S. Patil, D. K. Gautam, Optics Communications **201**, 413 (2002).
[18] T. Nakamura, K. Katayama, H. Mori, S. Fujiwara, Phys. Stat. Sol. (b) **241**(12), 2659 (2004).
[19] S. Venkatachalam, R. T. Rajendra Kumar, D. Mangalaraj, Sa. K. Narayandass, Kyunghae Kim, Junsin Yi, Solid-State Electronics **48**, 2219 (2004).
[20] Yuji Araki, Koji Ohkuno, Takeshi Furukawa, Junji Saraie, Journal of Crystal Growth **301**–**302**, 809 (2007).
[21] S. V. Ivanov, E. V. Lutsenko, S. V. Sorokin, I. V. Sedova, S. V. Gronin, A. G. Voinilovich, N. P. Tarasuk, G. P. Yablonskii, P. S. Kop'ev, Journal of Crystal Growth **311**, 2120 (2009).
[22] P. Gashin, A. Focsha, T. Potlog, A. V. Simashkevich, V. Leondar, Solar Energy Materials and Solar Cells **46**, 323 (1997).
[23] F. Engelhardt, L. Bornemann, M. Koentges, Th. Meyer, J. Parisi, E. Pschorr-Schoberer, B. Hahn, W. Gebhardt, W. Riedl, U. Rau, Progress in Photovoltaics: Research and

Applications **7**, 423 (1999).
[24] D. C. Cheng, H. C. Hao, M. Zhang, W. Shi, M. Lu, Nanoscale Research Letters **8**, 291 (2013).
[25] M. A. Olopade, O. O. Oyebola, B. S. Adeleke, Advances in Applied Science Research **3**(6), 3396 (2012).
[26] A. Rumberg, Ch. Sommerhalter, M. Toplak, A. Jager-Waldau, M. Ch. Lux-Steiner, Thin Solid Films **361-362**, 172 (2000).
[27] P. Saikia, P. K. Saikia, D. Saikia, Optoelectron. Adv. Mat. **5**(3), 204 (2011).
[28] R. B. Kale, C. D. Lokhande, Materials Research Bulletin **39**, 1829 (2004).
[29] C. Natarajan, M. Sharon, C. Levy - Clement, M. Neumann, Thin Solid Films **237**, 118 (1994).
[30] K. R. Murali, S. Dhanapandiyana, C. Manoharana, Chalcogenide Letters **6**(1), 51 (2009).
[31] D. Saravanakkumar, M. Kashif, V. Rethinasami, B. Ravikumar, S. Ppandiarajan, A. Ayeshamariam, A. Sivaranjani, M. Bououdina, S. Ramalingam, Journal of Ovonic Research **10**(5), 175 (2014).
[32] T. Yao, M. Ogura, S. Matsuoka, T. Morishita, Appl. Phys. Lett. **43**, 499 (1983).
[33] V. Mittal, N. P. Sessions, J. S. Wilkinson, G. S. Murugan, Optical Materials Express **7**(3), 713.
[34] I. Langmuir, Phys. Rev. **2**, 329 (1913).
[35] K. L. Chopra, Thin Film Phenomena, Mc Graw-Hill, New York, 1969.
[36] Y. Sirotin, M. Shaskolskaya, Fundamental of Crystal Physics, Moscow, Mir Publishers, 1982.
[37] Standart X-ray Diffraction Powder Patterns, National Bureau of Standarts Circular 539, Volume **III**, Issued June 10, 1954.
[38] Standart X-ray Diffraction Powder Patterns, National Bureau of Standarts Circular 539, Volume **II**, Issued June 15, 1953.
[39] K. T. Jacob, Shubhra Raj, L. Rannesh, International Journal of Materials Research **98**, 9 (2007).
[40] K. Hayashi, N. Sawaki, I. Akasaki, Japanese Journal of Applied Physics **30**(3), 501 (1991).
[41] Y. Kanemitsu, A. Yamamoto, H. Matsue, Y. Masumoto, Appt. Phys. Lett. **60**(11), (1992).
[42] B. H. Xu, Y. Liang, Z. Liu, X. Zhang, S. Hark, Adv. Mater. **20**, 3294 (2008).
[43] D. Nesheva, M. J. Scepanovic, S. Askrabic, Z. Levi, I. Bineva, Z. V. Popovic, Acta Physica Polonica A **116**(1), 75 (2009).
[44] T. M. Khan, M. F. Mehmood, A. Mahmood, A. Shah, Q. Raza, A. Iqbal, U. Aziz, Thin Solid Films **519**, 5971 (2011).
[45] H. X. Chuo, T. Y. Wang, W. G. Zhang, Journal of Alloys and Compounds **606**, 231 (2014).
[46] L. Agarwal, P. Agarwal, Journal of Electronic Materials **44**(10), (2015).
[47] R. G. Valeev, E. A. Romanov, V. L. Vorobiev, V. V. Mukhgalin, V. V. Kriventsov, A. I. Chukavin, B. V. Robouch, Mater. Res. Express **2**, 025006 (2015).
[48] Y. Alghamdi, Materials Sciences and Applications **8**, 726 (2017).
[49] A. Deneuville, D. Tanner, P. H. HollowayPhysical Review B **43**(8), 6544 (1991).
[50] J. Schneidert, R. D. Kirbyt, Physical Review B **6**(4),1290 (1972).
[51] Y. C. Cheng, C. Q. Jin, F. Gao, X. L. Wu, W. Zhong, S. H. Li, P. K. Chu, Journal of Applied Physics **106**, 123505 (2009).
[52] J. Díaz-Reyes, R. Castillo-Ojeda, J. Martínez-Juárez, O. Zaca-Moran, J. E. Flores-Mena, M. Galván -Arellano, International Journal of Circuits, Systems and Signal Processing **8**, (2014).
[53] G Irmer, E Monaico, I. M. Tiginyanu, G. Gartner, V. V. Ursaki, G. V. Kolibaba, D. D. Nedeoglo, J. Phys. D: Appl. Phys. **42**, 045405 (2009).
[54] T. Basak, M. N. Rao, S. L. Chaplot, Nilesh Salke, R. Rao, R. Dhanasekaran, A. K. Rajarajan, S. Rols, R. Mittal, V. B. Jayakrishnan, P. U. Sastry, Physica B **433**, 149 (2014).